Transportation Research Part B 46 (2012) 1159–1176

Contents lists available at SciVerse ScienceDirect

Transportation Research Part B

journal homepage: www.elsevier.com/locate/trb

On the stability of traffic perimeter control in two-region urban cities

Jack Haddad, Nikolas Geroliminis *

École Polytechnique Fédérale de Lausanne (EPFL), School of Architecture, Civil and Environmental Engineering (ENAC), Urban Transport Systems Laboratory (LUTS), Lausanne, Switzerland

ARTICLE INFO

Article history:
Received 20 August 2011
Received in revised form 13 April 2012
Accepted 13 April 2012

Keywords:
Stability characterization
Macroscopic fundamental diagram
State-feedback control
Traffic congestion

ABSTRACT

In this paper, stability analysis of traffic control for two-region urban cities is treated. It is known in control theory that optimality does not imply stability. If the optimal control is applied in a heavily congested system with high demand, traffic conditions might not change or the network might still lead to gridlock. A city partitioned in two regions with a Macroscopic Fundamental Diagram (MFD) for each of the regions is considered. Under the assumption of triangular MFDs, the two-region MFDs system is modeled as a piecewise second-order system. Necessary and sufficient conditions are derived for stable equilibrium accumulations in the undersaturated regimes for both MFDs. Moreover, the traffic perimeter control problem for the two-region MFDs system is formulated. Phase portraits and stability analysis are conducted, and a new algorithm is proposed to derive the boundaries of the stable and unstable regions. Based on these regions, a state-feedback control strategy is derived. Trapezoidal shape of MFDs are also addressed with numerical solutions.

1. Introduction

Monitoring and controlling congestion in arterial networks still remains a challenge. The issue is not only that the existing monitoring infrastructure in arterials is less dense than freeways but also that arterial systems traffic dynamics are more complex than these of freeways. The main reasons are the sharp changes of capacity (periodicity of green and red phases in short time intervals) and the characteristics of route choice (in arterials vehicles can randomly turn at intersections, search for parking, and begin or finish their trips in the middle of the street, which is not the case in freeways). If a vehicle is tracked on a freeway for 15 s we can estimate with high accuracy the speed field in the time-space proximity of the vehicle. Instead, this is not the case in arterials as there are strong variations in speeds and densities even for vehicles traveling in the same link during the same cycle length. This makes the control of traffic in urban regions more challenging than freeway systems.

Consider now a large urban traffic network at a specific point in time where congestion is unevenly distributed over space (like taking a photograph from a plane). This uneven congestion distribution occurs because of spatial inhomogeneity in demand, road infrastructure, and control. Recent studies Geroliminis and Sun (2011), Mazloumian et al. (2010), Daganzo et al. (2011) have shown that networks with heterogeneous distribution of density exhibit network flows smaller than those that approximately meet homogeneity conditions (low spatial variance of link density), especially for high network densities. Also, note that the scalability of flows from a series of links to large traffic networks is not a direct transformation. Route or network capacity can be significantly smaller than the capacity of a single link, because of the correlations between successive arterial links and the effect of offsets, Daganzo and Geroliminis (2008) and Boyacı and Geroliminis (2011). In case of long links, these effects are negligible and the physics of traffic much simpler. Nevertheless, most of congestion occurs in the city centers with dense topology of short links.

* Corresponding author. Address: GC C2 389, Station 18, 1015 Lausanne, Switzerland. Tel.: +41 21 6932481; fax: +41 21 6935060.
E-mail address: nikolas.geroliminis@epfl.ch (N. Geroliminis).

0191-2615/$ - see front matter © 2012 Elsevier Ltd. All rights reserved.
http://dx.doi.org/10.1016/j.trb.2012.04.004

The physical tool to advance this research is the Macroscopic Fundamental Diagram (MFD) of urban traffic, which provides for different network regions a unimodal, low-scatter relationship between network vehicle density [veh/km] and network space-mean flow [veh/h]. The first theoretical proposition of such a physical model was developed by Godfrey (1969), while similar approaches were also initiated by Herman and Prigogine (1979) and Daganzo (2007). The physical model of MFD was observed with dynamic features in congested urban networks in Yokohama by Geroliminis and Daganzo (2008). Network flow increases with density up to a critical point, while additional vehicles in the network cause strong reductions in flow. This work showed (i) that some urban regions approximately exhibit an MFD, (ii) there is a robust linear relation between the regions average flow and rate vehicles reach their destinations (outflow) and (iii) the shape of the MFD is not very sensitive to different demand patterns. Property (i) is important for modeling purposes as details in individual links are not needed to describe the congestion level of cities and its dynamics. Property (ii) is important for monitoring purposes as flow can be easily observed with different types of sensors while outflow is more difficult. Property (iii) is important for control purposes as efficient active traffic management schemes can be developed without a detailed knowledge of O–D tables. MFD can also be utilized to introduce simple control strategies to improve mobility in homogeneous city centers. The main logic of the strategies is that they aim to decrease inflows in regions with points in the decreased part of an MFD, and manage the accumulation to maintain the flow in the city on its maximum. The optimal control policy was derived for a single MFD system in Daganzo (2007). Nevertheless, the derived policy might not be optimal if vehicles have destinations outside the center of the city, or the periphery of the region has limited storage and might gridlock. Other investigations of MFD using empirical or simulated data can be found in Buisson and Ladier (2009), Ji et al. (2010), Mazloumian et al. (2010), Courbon and Leclercq (2011), Laval (2010) and others.

An important observation (see for example Kalman, 1960) is that optimality does not imply stability. If the optimal control is applied in a heavily congested system with high demand, traffic conditions might not change or the network might still lead to gridlock.

Stability analysis and control synthesis of a nonlinear system are not trivial tasks. Even for a simple class of nonlinear system such as piecewise affine systems, and despite the fact that piecewise affine models are just a composition of linear dynamic systems, their stability properties are complex and cannot be easily deduced from those of the component linear subsystems, and instead, numerical tests were proposed in Bemporad et al. (2000).

In this paper, the stability analysis for two-region MFDs system is treated. Briefly speaking an urban region can have a well-defined MFD (low scatter) (i) if the variance of link density is small (network roughly homogeneous) and (ii) topography of network is redundant (many options for route choices that can facilitate (i)) (see Daganzo and Geroliminis, 2008; Mazloumian et al., 2010; Geroliminis and Sun, 2011). Thus, by minimizing link density variance, this can imply an MFD with low scatter. Small variance is also important because as Mazloumian et al. (2010) showed, for the same average density, network flow is smaller in case of higher density variance. In a similar manner, Daganzo et al. (2011) showed for networks of two overlapping bins that symmetric equilibrium patterns with equal flows and densities across all links are unstable if the network density is high and can create states much below than an idealized MFD with homogeneous densities in all links. A city can be partitioned in a number of regions with low-scatter MFDs (Ji and Geroliminis, 2011). Then, perimeter control strategies can be developed to maximize mobility for multi-region cities. In this paper we assume well-defined MFDs and analyze the stability of traffic perimeter control, e.g. the paper identifies the unstable control conditions where the network will lead to gridlock and cannot be prevented by any control strategy.

The dynamic equations are formulated as a piecewise second-order system. The MFDs are assumed to be in triangular shapes, and each region can have two types of demand, endogenous and exogenous. In this paper we analyze cases where one of the two regions is the center of attraction and does not generate exogenous demand. The first part of the paper focuses on systems where all trips have destination in the center of the city (2 degrees of demand), while the second part allows some trips from the external region to remain in the external region (3 degrees of demand). Furthermore, necessary and sufficient conditions are derived for asymptotically stable equilibrium point in the undersaturated regimes for both MFDs. A new algorithm is proposed for computing the boundaries of stable and unstable regions and a state-feedback control is derived where the criterion is to maximize the output of the system, i.e. the number of vehicles that complete their trips and reach their destinations. We also investigate how a trapezoidal MFD affects the shape of the stability region.

This paper is organized as follows: the dynamic equations and the control problem for two-region MFDs system are formulated in Section 2.1, and phase portrait for piecewise second-order system is constructed in Section 2.2. In Section 3 the stability analysis is conducted and the new algorithm for computing the boundaries of the stable and unstable regions is proposed. The state-feedback control law is derived in Section 4. Numerical results for region of attraction for three degrees of demand are presented in Section 5.

2. Two-state, two-region MFDs system

2.1. Dynamic equations and problem formulation

Let us consider a traffic urban network that is partitioned to two regions, $i = 1, 2$, where each region has an MFD, e.g. a city with two regions: the periphery of the center (1) and the city center (2). Assume that the partitioned network has only two

demands: $q_1(t)$ [veh/s] is the exogenous traffic demand generated in region 1 with destination to region 2 at time t, while $q_2(t)$ [veh/s] is the endogenous traffic demand generated in region 2 with destination to region 2 at time t (we will relax this assumption later). Moreover, assume that a perimeter control $u(t)$ [–] exists on the border between the two regions, where $0 \leqslant u(t) \leqslant 1$. The control may restrict the flow that transfers from region 1 to 2, e.g. if $u(t) = 0$ then the control prevents any vehicle to transfer from region 1 to 2. The perimeter control can be actuated in different ways, e.g. by coordinating green and red durations of signalized intersections placed on the border between two regions, or with dynamic pricing schemes.

Two state variables are used to model the dynamics of the traffic urban network with two demands according to the MFDs of both regions. The two state variables are the *accumulations* $n_i(t)$ [veh], $i = 1, 2$, defined as the total number of vehicles in region i at time t. Under the assumption that average trip length within each region is constant with time, the MFD links accumulation $n_i(t)$ and *trip completion flow* $G_i(n_i(t))$ [veh/s], defined as the uncontrolled or unrestricted rate of vehicles that reach their destinations, Geroliminis and Daganzo (2008). For the two-state two-region system, since the perimeter control $u(t)$ may restrict vehicles to transfer from region 1 to 2, then only a portion of vehicles $G_1(n_1(t)) \cdot u(t)$ can actually transfer from region 1 to 2. However, there is no restriction on the trip completion flow from region 2 to 2.

We now assume that the demands are constant with time, i.e. $q_i(t) = q_i$, $i = 1, 2$. Time-dependent demand profiles will be discussed later. Then the *two-state two-region MFDs control problem* is formulated as follows: given initial state accumulations $n_{1,0}$, $n_{2,0}$, end state accumulations $n_{1,f}$, $n_{2,f}$, and control time horizon $[0, t_f]$, find the optimal control policy that maximizes the number of vehicles reach their destinations, i.e.

$$J = \max \int_0^{t_f} G_2(n_2(t))\mathrm{d}t \tag{1}$$

subject to

$$\frac{\mathrm{d}n_1(t)}{\mathrm{d}t} = q_1 - G_1(n_1(t)) \cdot u(t), \tag{2}$$

$$\frac{\mathrm{d}n_2(t)}{\mathrm{d}t} = q_2 + G_1(n_1(t)) \cdot u(t) - G_2(n_2(t)), \tag{3}$$

$$n_1(0) = n_{1,0}; \quad n_2(0) = n_{2,0}, \tag{4}$$

$$n_1(t_f) = n_{1,f}; \quad n_2(t_f) = n_{2,f}, \tag{5}$$

$$0 < u_{\min} \leqslant u(t) \leqslant u_{\max} < 1, \tag{6}$$

where $u_{\min}$ and $u_{\max}$ are a priori given lower and upper bounds of the perimeter control, and Eqs. (2), (3) are the conservation of mass equations for $n_1(t)$ and $n_2(t)$, respectively. The criterion is to maximize the output of the traffic network, i.e. the number of vehicles that complete their trips and reach their destinations. For the defined demands in a two-region MFDs system, there is only one destination which is region 2, hence the maximum number of vehicles reach their destination is defined in (1). Note that the control time horizon t_f is assumed to be large enough to reach the a priori known end state point.

The trip completion flows of the two regions depend on their MFD shapes. In this paper, the MFDs for both two regions, e.g. the city center and the periphery of the city, are assumed to be triangular, see Fig. 1, with capacity γ_i [veh/s] at critical accumulation $n_{i,\mathrm{cr}}$ [veh], and jam accumulation $n_{i,\mathrm{jam}}$ [veh]. Two traffic regimes are distinguished in a triangular shape of MFD: uncongested $0 \leqslant n_i(t) \leqslant n_{i,\mathrm{cr}}$ and congested $n_{i,\mathrm{cr}} \leqslant n_i(t) \leqslant n_{i,\mathrm{jam}}$. The triangular shape is defined as a piecewise affine function

$$G_i(n_i(t)) = \begin{cases} \frac{\gamma_i}{n_{i,\mathrm{cr}}} \cdot n_i(t) & \text{if } 0 \leqslant n_i(t) \leqslant n_{i,\mathrm{cr}}, \\ \frac{-\gamma_i}{n_{i,\mathrm{jam}} - n_{i,\mathrm{cr}}} \cdot n_i(t) + \frac{\gamma_i \cdot n_{i,\mathrm{jam}}}{n_{i,\mathrm{jam}} - n_{i,\mathrm{cr}}} & \text{if } n_{i,\mathrm{cr}} \leqslant n_i(t) \leqslant n_{i,\mathrm{jam}}. \end{cases} \tag{7}$$

Substituting (7) into the dynamic Eqs. (2) and (3), one gets a piecewise second-order system of two state variables $n_1(t)$ and $n_2(t)$ with four *state regions*, see also Fig. 1:

- state region I, for $0 \leqslant n_1(t) \leqslant n_{1,\mathrm{cr}}$ and $0 \leqslant n_2(t) \leqslant n_{2,\mathrm{cr}}$,
- state region II, for $0 \leqslant n_1(t) \leqslant n_{1,\mathrm{cr}}$ and $n_{2,\mathrm{cr}} \leqslant n_2(t) \leqslant n_{2,\mathrm{jam}}$,
- state region III, for $n_{1,\mathrm{cr}} \leqslant n_1(t) \leqslant n_{1,\mathrm{jam}}$ and $0 \leqslant n_2(t) \leqslant n_{2,\mathrm{cr}}$,
- state region IV, for $n_{1,\mathrm{cr}} \leqslant n_1(t) \leqslant n_{1,\mathrm{jam}}$ and $n_{2,\mathrm{cr}} \leqslant n_2(t) \leqslant n_{2,\mathrm{jam}}$.

2.2. Phase portraits for piecewise second-order system

In order to investigate the behavior of the two-state two-region MFDs system (2)–(6), a phase portrait is constructed by plotting trajectories from a large number of initial states spread all over the (n_2, n_1)-plane with constant control u. The *qualitative behavior* of the trajectories near equilibrium points can be also determined via linearization with respect to these points, see e.g. Khalil (2002), Sastry (1999).

The equilibrium points, i.e. $\mathrm{d}n_i/\mathrm{d}t = 0$, $i = 1, 2$, in state regions I, II, III, and IV, after substituting (7) into (2) and (3) are

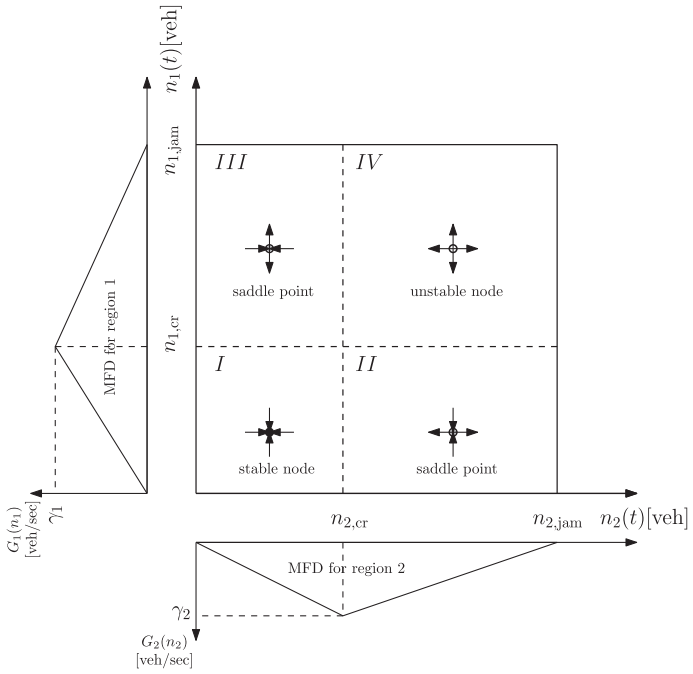

Fig. 1. Four state regions I, II, III, and IV in (n_2, n_1)-plane according to triangular MFDs with a different type of equilibrium points.

$$(n_{2,\text{eq}}, n_{1,\text{eq}})_I = \left(\frac{(q_1+q_2)\cdot n_{2,\text{cr}}}{\gamma_2}, \frac{q_1 \cdot n_{1,\text{cr}}}{\gamma_1 \cdot u}\right), \tag{8}$$

$$(n_{2,\text{eq}}, n_{1,\text{eq}})_{II} = \left(n_{2,\text{jam}} - \frac{(n_{2,\text{jam}} - n_{2,\text{cr}})\cdot (q_1+q_2)}{\gamma_2}, \frac{q_1 \cdot n_{1,\text{cr}}}{\gamma_1 \cdot u}\right), \tag{9}$$

$$(n_{2,\text{eq}}, n_{1,\text{eq}})_{III} = \left(\frac{(q_1+q_2)\cdot n_{2,\text{cr}}}{\gamma_2}, n_{1,\text{jam}} - \frac{q_1 \cdot (n_{1,\text{jam}} - n_{1,\text{cr}})}{\gamma_1 \cdot u}\right), \tag{10}$$

$$(n_{2,\text{eq}}, n_{1,\text{eq}})_{IV} = \left(n_{2,\text{jam}} - \frac{(n_{2,\text{jam}} - n_{2,\text{cr}})\cdot (q_1+q_2)}{\gamma_2}, n_{1,\text{jam}} - \frac{q_1 \cdot (n_{1,\text{jam}} - n_{1,\text{cr}})}{\gamma_1 \cdot u}\right). \tag{11}$$

Proposition 1. *The necessary and sufficient conditions for equilibrium points, i.e. $dn_i/dt = 0$, $i = 1, 2$, in state regions I, II, III, and IV of the two-state two-region MFDs system with triangular shapes are:*

$$q_1 + q_2 < \gamma_2, \tag{12}$$

$$q_1 < \gamma_1 \cdot u. \tag{13}$$

Proof. If $dn_i/dt = 0$ for $i = 1, 2$ hold, then they imply (8)–(11), and by definition the equilibrium points in state regions I, II, III, and IV, i.e. $(n_{2,\text{eq}}, n_{1,\text{eq}})_I$, $(n_{2,\text{eq}}, n_{1,\text{eq}})_{II}$, $(n_{2,\text{eq}}, n_{1,\text{eq}})_{III}$, and $(n_{2,\text{eq}}, n_{1,\text{eq}})_{IV}$ satisfy the lower and upper bounds of their regions, i.e. $0 \leqslant n_1(t) \leqslant n_{1,\text{cr}}$ and $0 \leqslant n_2(t) \leqslant n_{2,\text{cr}}$ for state region I, and so on. Substituting each equilibrium point in the lower and upper bounds for its state region, one gets (12) and (13).

Clearly, if (12) and (13) hold, then each equilibrium point satisfies the lower and upper bounds for its region, i.e. there exist equilibrium points (8)–(11) such that they belong to state regions I–IV, respectively. □

If (12) or (13) does not hold, then all trajectories reach at least one jam accumulation and the traffic network leads to gridlock, if demand continues to be constant.

Let us rewrite (2) and (3), respectively, as

$$\frac{dn_1(t)}{dt} = f_1(n_1, n_2), \tag{14}$$

$$\frac{dn_2(t)}{dt} = f_2(n_1, n_2), \tag{15}$$

where $f_1(n_1,n_2) = q_1 - G_1(n_1(t)) \cdot u(t)$, $f_2(n_1,n_2) = q_2 + G_1(n_1(t)) \cdot u(t) - G_2(n_2(t))$. Let us assume that there exists at least one equilibrium point, denoted by $n_{1,eq}$, $n_{2,eq}$, for (14) and (15), i.e. $dn_i/dt = 0$, $i = 1, 2$, then the Jacobian matrix of (14) and (15) at $n_{1,eq}$, $n_{2,eq}$

$$A = \left[\begin{array}{cc} \frac{\partial f_1}{\partial n_1} & \frac{\partial f_1}{\partial n_2} \\ \frac{\partial f_2}{\partial n_1} & \frac{\partial f_2}{\partial n_2} \end{array}\right]\Bigg|_{n_1=n_{1,eq},n_2=n_{2,eq}}. \tag{16}$$

Hence, under the assumption that (12) and (13) hold and for a given constant u, one can calculate the Jacobian matrix at the equilibrium points in the state regions I, II, III, and IV according to

$$\begin{aligned} A_I &= \left[\begin{array}{cc} -\frac{\gamma_1}{n_{1,cr}} \cdot u & 0 \\ \frac{\gamma_1}{n_{1,cr}} \cdot u & -\frac{\gamma_2}{n_{2,cr}} \end{array}\right] \qquad A_{II} = \left[\begin{array}{cc} -\frac{\gamma_1}{n_{1,cr}} \cdot u & 0 \\ \frac{\gamma_1}{n_{1,cr}} \cdot u & \frac{\gamma_2}{n_{2,jam}-n_{2,cr}} \end{array}\right] \\ A_{III} &= \left[\begin{array}{cc} \frac{\gamma_1}{n_{1,jam}-n_{1,cr}} \cdot u & 0 \\ -\frac{\gamma_1}{n_{1,jam}-n_{1,cr}} \cdot u & -\frac{\gamma_2}{n_{2,cr}} \end{array}\right] \quad A_{IV} = \left[\begin{array}{cc} \frac{\gamma_1}{n_{1,jam}-n_{1,cr}} \cdot u & 0 \\ -\frac{\gamma_1}{n_{1,jam}-n_{1,cr}} \cdot u & \frac{\gamma_2}{n_{2,jam}-n_{2,cr}} \end{array}\right]. \end{aligned} \tag{17}$$

The type of the equilibrium points is determined according to the eigenvalues of matrices A_I, A_{II}, A_{III}, and A_{IV} in (17), see Khalil (2002), Sastry (1999). All these matrices are lower triangular matrices, hence, the eigenvalues are the elements in the diagonal. The equilibrium point in region I is an asymptotically *stable equilibrium node* since the two eigenvalues are negative, the equilibrium points in regions II and III are *unstable saddle points* since one of the eigenvalues is positive and the other is negative, and the equilibrium point in region IV is an *unstable node* since both eigenvalues are real positive, i.e. $\gamma_1/(n_{1,jam} - n_{1,cr}) \cdot u > 0$ and $\gamma_2/(n_{2,jam} - n_{2,cr}) > 0$. The type of the equilibrium points are shown schematically in Fig. 1.

The phase portraits are numerically constructed according to the following steps under the assumption that (i) the necessary and sufficient conditions (12) and (13) hold and (ii) $u(t) = u$ is constant and a priori given during the construction of the portraits,

1. Calculate all equilibrium points according to (8)–(11).
2. Select a bounding box in the (n_2,n_1)-plane as

$$0 \leqslant n_1(t) \leqslant n_{1,jam}, \tag{18}$$

$$0 \leqslant n_2(t) \leqslant n_{2,jam}. \tag{19}$$

3. Calculate trajectories[1] for selected initial points: inside and near the bounding box (18) and (19), and near calculated equilibrium points in step 1.

Following these steps, the phase portraits are numerically conducted for example 1 as shown in Fig. 3a, where the green lines are the trajectories and the gray arrows are the direction of the trajectories. The equilibrium points in the four state regions are marked by circles in the (n_2,n_1)-plane. The input data for example 1 are as follows: the traffic demand rates are $q_1 = 0.194$ [veh/s], $q_2 = 0.069$ [veh/s], the perimeter control $u(t) = u_{max} = 0.8$, the MFD parameters are: $\gamma_1 = 0.5$ [veh/s], $n_{1,cr} = 50$ [veh], $n_{1,jam} = 200$ [veh], $\gamma_2 = 0.583$ [veh/s], $n_{2,cr} = 150$ [veh], $n_{2,jam} = 450$ [veh], i.e. region 2 is about twice as large as region 1. Values of these parameters are consistent with empirical observations from Geroliminis and Daganzo (2008).

3. Stability characterization of two-state two-region system

The phase portrait conducted in Section 2.2 shows that if (12) and (13) hold then some of the trajectories reach asymptotically an equilibrium point while other trajectories reach jam accumulation at least for one of the regions, e.g. see Fig. 3b. Hence, before solving the two-state two-region MFDs control problem, behavior and stability analysis of the two-region system are conducted. We define now a stable region and a region of attraction for the phase portraits.

According to Section 2.2, if the necessary and sufficient conditions (12) and (13) hold, then one stable equilibrium point exists in state region I. *Stable trajectories* are defined as trajectories that approach a stable equilibrium point in state region I $(n_{2,eq},n_{1,eq})_I$ correspond to $u(t)$ as $t \to t_f$,[2] see (8), while *unstable trajectories* approach at least one jam accumulation, i.e. $n_1(t_f) = n_{1,jam}$ or/and $n_2(t_f) = n_{2,jam}$, and there exists no control $u(t)$, even a time dependent one, that can bring trajectories to stable equilibrium point under the prevailing traffic demand. Moreover, a *stable region* is defined as the set of all points that have stable trajectories, while all other points with unstable trajectories define an *unstable region*.

To construct the stable region, we need to start from an easier problem. Thus, a *region of attraction* for constant control $u(t) = u$, denoted by RA_u, is defined as the set of all points (n_2,n_1) that their trajectories are stable with applied control u. Finding the region of attraction of a nonlinear system is a significant research topic that has been studied extensively, e.g. Chiang and Thorp (1989), Mhaskar et al. (2006), Tan and Packard (2008), Topcu and Packard (2009). Since computing the exact RA is

[1] Computer programs for solving ordinary differential equations are widely available. In this paper, Simulink, the simulation tool of MATLAB is used.

[2] It is assumed that t_f is large enough to reach asymptotically the equilibrium point.

hard, researchers have focused on finding Lyapunov functions whose sublevel sets provide invariant subsets of the RA. There is no general Lyapunov function that may apply for nonlinear systems, therefore, different methods were presented for specific class of nonlinear systems, e.g. piecewise quadratic Lyapunov functions and linear matrix inequalities approach have been proposed in Hassibi and Boyd (1998) and Johansson and Rantzer (1998) for piecewise affine systems. It is a hard task to find a Lyapunov function for *bilinear systems*, which is a class of nonlinear control systems where the control u is act as an additive and multiplicative coefficient of state variables, Elliott (2009). Moreover, it was concluded in Gutman (1981) that there exists no general method to design stabilizing controllers for bilinear system. The two-state two-region system is even more sophisticated than bilinear system since it is a *piecewise bilinear system*, see (2), (3), and (7), however, a new algorithm is proposed to calculate the region of attraction according to analytical and numerical computations. Regions of attraction (RA*s*) are used to characterize the stable and unstable regions in this section, and to design a state-feedback control in Section 4.

3.1. Region of attraction boundary

Since the two-region MFDs system is piecewise system, and has an equilibrium point in each piece (state region), three different cases are distinguished to calculate the region of attraction boundary.

Recall that the dynamic behavior around the equilibrium points is *locally* described for each state region according to their types as isolated points in the (n_2, n_1)-plane as shown in Fig. 1. However, calculating region of attraction boundary for the four state regions, the trajectories' behaviors are described as the superposition of the dynamic behaviors caused by two or more equilibrium points. Therefore, according to the distances between the positions of equilibrium points in the plane, see (8)–(11), the superposition of dynamic behaviors is different, resulting in three different cases of regions of attraction: cases a, b, and c. The region of attraction boundaries for constant control for cases a, b, and c are schematically shown in Fig. 2. In case a, the equilibrium points in state regions III and IV are "far" enough from each other such that trajectories do not interfere each other, i.e. the type of equilibrium points and the qualitative behavior near them are maintained as two isolated points in the plane, see Fig. 1. In case b and c, the two equilibrium points in regions II and III affect points near them such that the speed and direction of trajectories pass through them are a superposition result of direction and speed responses from equilibrium point II and III. Therefore, the behavior of trajectories and the boundary in cases b and c are different than that in case a. In case a, the attraction boundary passes through state region IV and its equilibrium point. In case b, the boundary passes through state region IV, while it passes through state region I in case c. Intuitively speaking, cases a and b show that even if initial conditions are congested (regions II, III, and IV) there exists some control u, that can lead the system to a stable uncongested equilibrium. This can be the case in the offset of congestion. If demand is very high, the region of attraction will shrink (case c) and demand has to decrease to allow the system to reach a stable uncongested equilibrium and avoid gridlock.

Under the assumption that $u(t)$ is constant during the control time horizon, i.e. $u(t) = u$ for $[0, t_f]$, the following steps are presented for computing the RA boundary curve, see Fig. 2:

1. Calculate all equilibrium points according to (8)–(11).
2. Start from the saddle equilibrium point in state region II, and calculate the corresponding eigenvector of the negative eigenvalue of the linearized system in that region, i.e. $\lambda_1 = -\gamma_1/n_{1,\mathrm{cr}} \cdot u < 0$, according to

$$(n_2, n_1) = \left(1, \frac{-\gamma_2 \cdot n_{1,\mathrm{cr}}}{\gamma_1 \cdot u \cdot (n_{2,\mathrm{jam}} - n_{2,\mathrm{cr}})} - 1\right), \tag{20}$$

therefore, the slope of line AB is $-\gamma_2 \cdot n_{1,\,\mathrm{cr}}/(\gamma_1 \cdot u \cdot (n_{2,\mathrm{jam}} - n_{2,\mathrm{cr}})) - 1$.

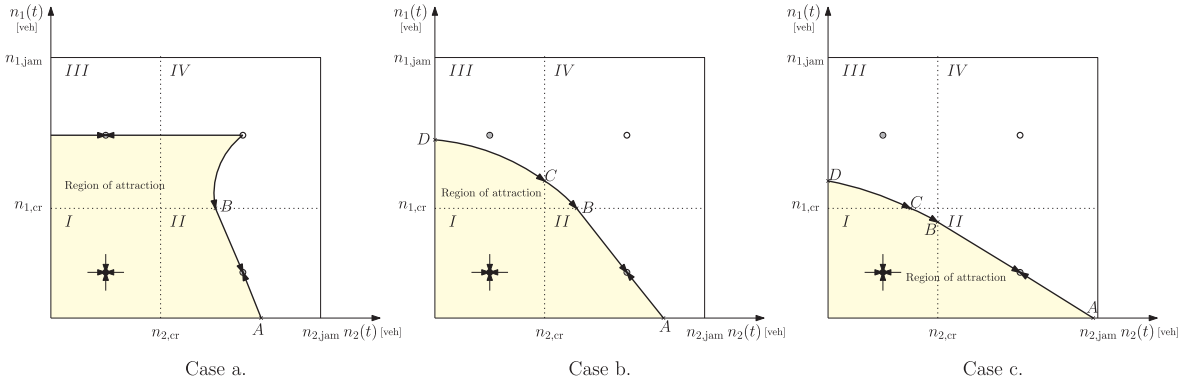

Fig. 2. Region of attraction corresponds to constant control u: cases a, b, and c.

3. Given the slope of the line AB and the saddle equilibrium point $(n_{2,eq}, n_{1,eq})_{II}$, extend the line in both direction until hitting the boundaries of region II. Depending on the value of the slope, point B might intersect with line $n_1(t) = n_{1,cr}$ or $n_2(t) = n_{2,cr}$.
4. If point B intersects with $n_2(t) = n_{2,cr}$, then it is case c. Calculate the trajectory from points B to C (region I) and C to D (region III) in reverse way according to Appendix A.3.
5. If point B intersects first with $n_1(t) = n_{1,cr}$, then the trajectory enters region IV, and we need to calculate it in reverse direction starting from point B according to Eqs. (A.3), (A.4), and (A.5) in Appendix A.1, with initial state point B and $t = 0 \rightarrow \infty$. The solution in region IV might reach first unstable equilibrium point of region IV (case a) or intersect with line $n_2(t) = n_{2,cr}$ (case b):
   - Case a: draw a horizontal line staring from the unstable equilibrium point $(n_{2,eq}, n_{1,eq})_{IV}$ and moving through the saddle point $(n_{2,eq}, n_{1,eq})_{III}$ towards $n_2(t) = 0$. Note from (10) and (11) that equilibrium points in III and IV have the same value for $n_1(t)$.
   - Case b: calculate the trajectories from points B to C and C to D in reverse way, according to Appendix A.2.

Note that the RA boundary curve is combined from several trajectories some of them are calculated numerically, while others are calculated analytically, see Appendices A.1, A.2, and A.3.

The region of attraction boundaries for cases a, b, and c are demonstrated by examples 1, 2, and 3, as shown in Fig. 3a–c, respectively, where the red curve is the corresponding RA boundary to $u(t) = u_{max}$. The input data for example 1 is given in Section 2.2. The traffic demand rates for example 2 are $q_1 = 0.194$ [veh/s], $q_2 = 0.319$ [veh/s] and the perimeter control is $u(t) = u_{max} = 0.8$, while for example 3 the traffic demand rates are $q_1 = 0.194$ [veh/s], $q_2 = 0.278$ [veh/s] and the perimeter control is $u(t) = u_{max} = 1$. The MFD parameters for examples 2 and 3 are the same as for example 1.

Until this section, the RA boundaries for all numerical examples 1, 2, and 3 were calculated for constant control $u(t) = u_{max}$ (trajectories drawn by green color). Clearly, different RA boundaries and trajectories are obtained by applying $u(t) = u_{min}$, e.g. the corresponding phase portraits and RA boundary for example 1 to $u(t) = u_{min} = 0.45$ and $u(t) = u_{max} = 0.8$ are shown in Fig. 3d, where trajectories are drawn by blue color and the RA boundary by cyan color for u_{min}. Note that if the necessary conditions (12) and (13) are violated, the reader should refer to Remark 1 at a later section.

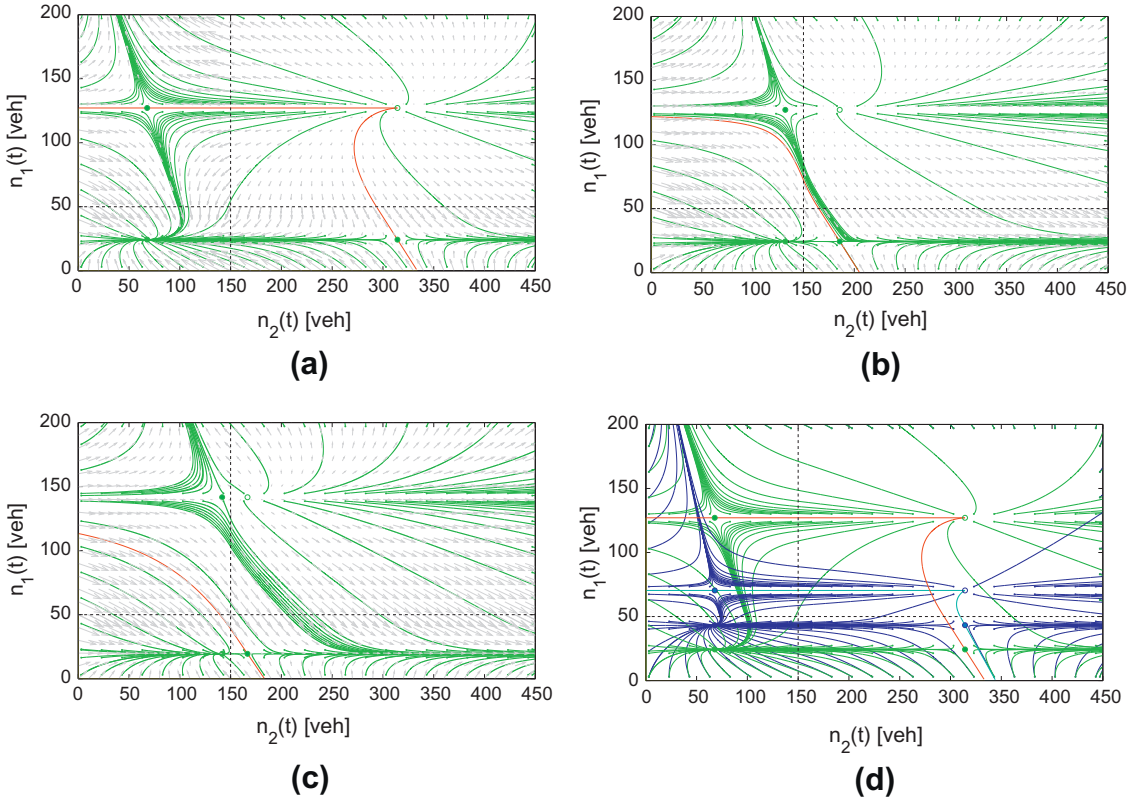

Fig. 3. (a) Numerical example 1 demonstrates case a; (b) numerical example 2 demonstrates case b; (c) numerical example 3 demonstrates case c; and, (d) numerical example 1 corresponds to $u(t) = u_{min}$ (trajectories in blue and RA boundary in cyan) and $u(t) = u_{max}$ (trajectories in green and RA boundary in red). (For interpretation of the references to colour in this figure legend, the reader is referred to the web version of this article.)

The three cases of the region of attraction boundaries shown in Fig. 2 correspond to triangular MFDs. The phase portraits approach can be also utilized to calculate the region of attraction boundary for more complex shapes than triangulares, e.g. trapezoidal shapes with several piecewise linear components, however more cases are expected as the boundary would pass through different state regions with different dynamic equations. Therefore, the five steps for computing the RA boundary curve presented in this section should be extended. The procedure will be similar but more tedious. Nevertheless, similar trajectories and boundary behaviors are expected for triangular and trapezoidal shapes of MFDs especially when the shapes are close to each other. The extensions for the five steps would be only technical as the piecewise second-order system of the two state variables $n_1(t)$ and $n_2(t)$ will have more state regions when both MFDs have trapezoidal shapes instead of triangular shapes. The extensions are not presented in this paper as they do not add extra information regarding the stability analysis for the two-state two-region system, however, numerical example 4 is presented to demonstrate the impacts of assuming trapezoidal shapes instead of triangular shapes for different values of capacities and control.

In numerical example 4, the boundaries of region of attraction are compared for four sets of triangulares with same $n_{i,\mathrm{cr}}$ and $n_{i,\mathrm{jam}}$ and value of capacity change as a fraction K, $K = 1, 0.72, 0.6, 0.48$, and one set of trapezoidal shapes of MFDs as shown in Fig. 4a. The MFDs for regions 1 and 2 are symmetric, but region 1 is twice larger with a capacity equal to K. The capacities of the trapezoidal MFDs are 0.48 and 0.24 [veh/s] for regions 1 and 2, respectively. The perimeter control for example 4 is $u(t) = 0.85$, while two levels of demands are analyzed a medium ($q_1 = 0.042$, $q_2 = 0.0278$ [veh/s]) and a higher level ($q_1 = 0.07$, $q_2 = 0.14$ [veh/s]). The results in Fig. 4b and c show that increasing the capacities of the triangular MFDs increases the region of attraction. It is also shown that the boundaries of the trapezoidal MFDs are close to the two boundaries of the triangular MFDs with $K = 0.6$ and $K = 0.72$. Note that in the $G(n)$ graph of Fig. 4a, when $K = 0.6$ the areas under both triangular and trapezoidal MFDs are similar, while for $K = 0.72$ the triangular MFDs envelop the trapezoidal MFDs having the same free flow speeds and backward wave speeds. These observations imply some guidance for choosing values of K for a triangular MFD to approximate a given trapezoidal MFD, however, calibration of K is out of the scope of this paper and this area of research should be investigated more deeply in the future.

3.2. Stability characterization

In Section 3.1, an algorithm is proposed to compute the RA_u boundary for a constant control u. In this section, this algorithm is applied to characterize the stable and unstable regions.

Recall that stable region is defined as the set of all points that have at least one trajectory, which approaches a corresponding stable equilibrium point for some control $u(t)$. If $u(t)$ is assumed to be constant for the whole control period, then the stable region is the set of all possible RA*s*. However, since the control may change over the control period, the stable region is wider, i.e. points outside the set of all RA*s* may also be stable if there exits at least one trajectory that enters the set of all RA*s*.

In principle, in order to characterize the stable region, one has to calculate RA*s* correspond to all constant u, that satisfy (6), and explore the state space for trajectories that enter these RA*s*. However, qualitative behavior and numerical examples show that computations of $\mathrm{RA}_{u_{\min}}$ and a few trajectories are enough to characterize the stable region boundary. The quantitative behavior of RA*s* for a wide range of u are shown in Fig. 5a and b for triangular and trapezoidal MFDs, respectively. The results shown in Fig. 5a are for numerical example 5 where its input data are the same as the input data of example 1 except q_2 is much larger, $q_2(t) = 0.347$ [veh/s], while the results shown in Fig. 5b are for example 4.

In the following, we restrict our explanations how to characterize the stable region for the two-state system to triangular MFDs. In case of trapezoidal MFDs, the same concept holds but extended explanations are needed as the RA_u boundary cases are different from cases a, b, and c.

From the quantitative and qualitative behavior of the RA*s* for triangular MFDs shown in Fig. 5a and Fig. 2, respectively, two different shapes of stable region are distinguished according to $\mathrm{RA}_{u_{\min}}$, see also Fig. 6: (i) $\mathrm{RA}_{u_{\min}}$ belong to case a, (ii) $\mathrm{RA}_{u_{\min}}$ belongs to case b or case c. The solid curve in Fig. 6 is a boundary that characterizes the stability region and splits (n_2, n_1)-plane into stable and unstable regions. Computing $\mathrm{RA}_{u_{\min}}$ and a few trajectories are enough to characterize the stable region boundary. For case a, the boundary is combined from (1) a horizontal trajectory that passes through the unstable saddle point according to $u_{\max}$ in state region III and ends at the unstable equilibrium point in state region IV according to $u_{\max}$, (2) a trajectory that is reversely calculated according to $u_{\min}$, denoted by $\tilde{u}_{\min}$ as shown in Fig. 6, starts from unstable equilibrium point in state region IV according to $u_{\max}$ and ends at the unstable equilibrium point in state region IV according to $u_{\min}$, and (3) the remaining part of $\mathrm{RA}_{u_{\min}}$ that passes through the unstable saddle point in state region II. For cases b and c, the boundary is combined from (1) a trajectory that starts from the horizontal axes with $u_{\max}$ and ends at a tangent point with $\mathrm{RA}_{u_{\min}}$, and (2) the remaining part of $\mathrm{RA}_{u_{\min}}$ that passes through the unstable saddle point in state region II, see Fig. 6. Numerical example 5 with upper and lower bounds $u_{\max} = 0.75$, $u_{\min} = 0.5$ demonstrates cases a, and with upper and lower bounds $u_{\max} = 0.75$, $u_{\min} = 0.6$ demonstrates cases b.

In Section 3.1, the RA boundary was analyzed for dynamic equations with constant demands q_1 and q_2, see (2) and (3). However, the same analysis can be also used for time varying demand $q_1(t)$ and $q_2(t)$, since for the dynamic Eqs. (2) and (3) no bifurcation happens with time varying demand, i.e. the difference in behavior around equilibrium points is quantitative but not qualitative when demand varies, it means that there will be always (if conditions (12) and (13) hold) one stable and one unstable equilibrium points in state regions I and IV, respectively, two saddle equilibrium points in regions II and III. Only the positions of the equilibria points varies within each region. The reason that no bifurcation happens with time

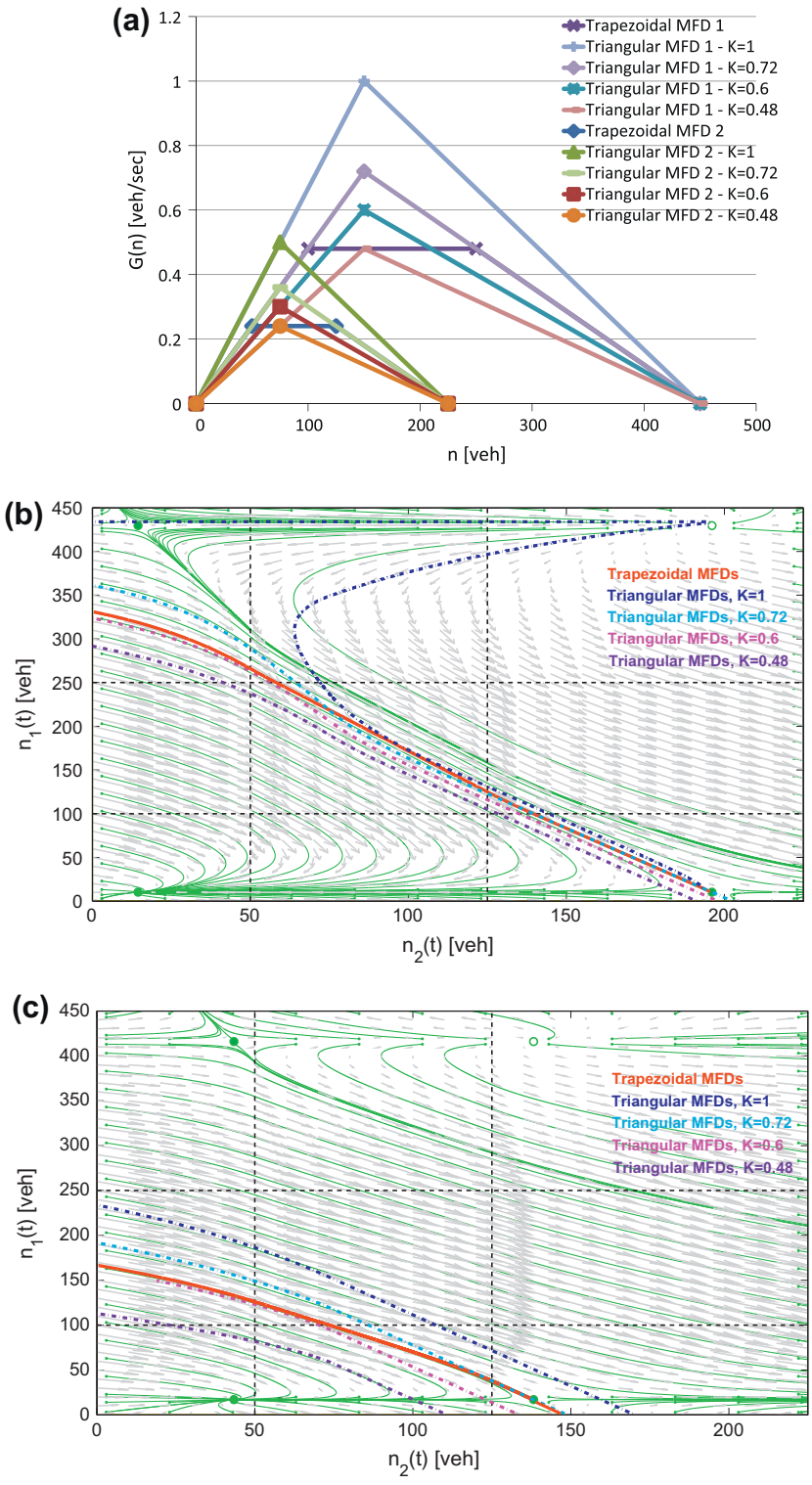

Fig. 4. Numerical example 4: (a) different triangular and trapezoidal shapes of MFDs; corresponding phase portraits to the trapezoidal shapes for (b) low demand and (c) higher demand, trajectories and region of attraction boundaries are drawn in green and red, respectively. Boundaries of region of attraction correspond to different triangular shapes $K = 1, 0.72, 0.6, 0.48$ are shown in dashed lines. (For interpretation of the references to colour in this figure legend, the reader is referred to the web version of this article.)

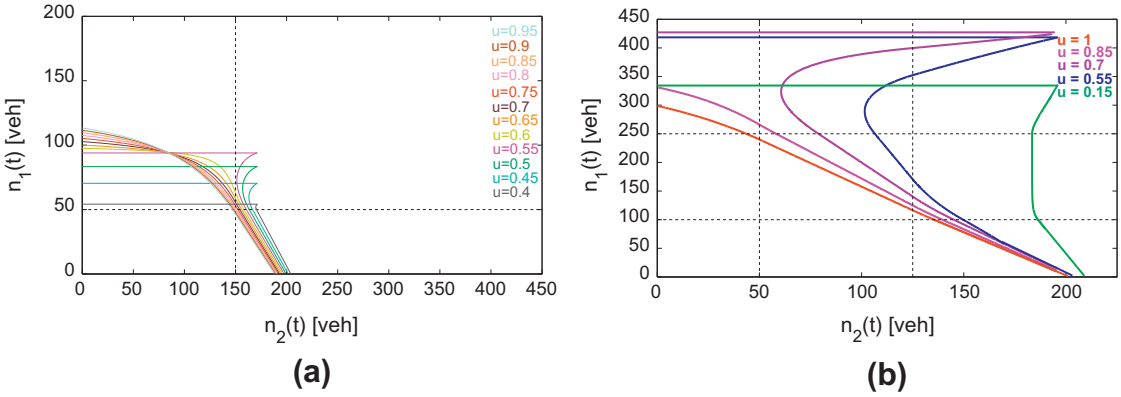

Fig. 5. RA*s* for wide range of u for (a) triangular MFDs in example 5, and (b) trapezoidal MFDs in example 4.

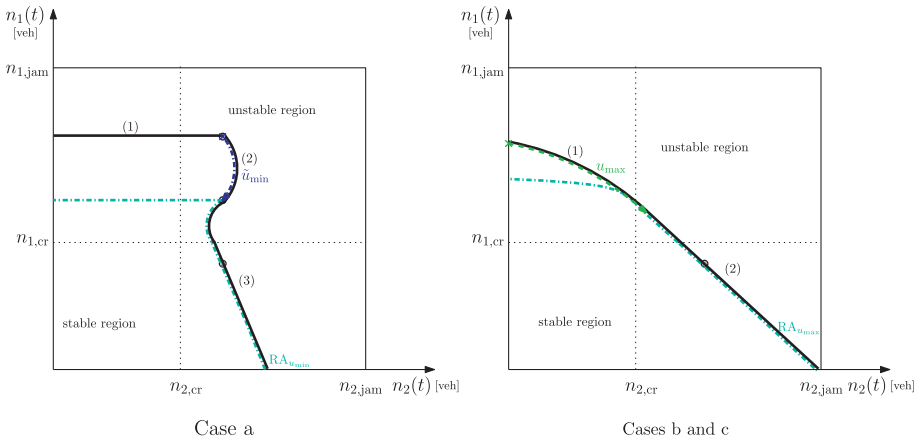

Fig. 6. Stable and unstable regions for cases a, b, and c.

varying demand is that each equilibrium point is a function of $q_1(t)$ and $q_2(t)$. Then, $n_{1,eq}(q_1(t),q_2(t))$, $n_{2,eq}(q_1(t),q_2(t))$ is a smooth function of $q_1(t)$, $q_2(t)$, as long as the Jacobian linearization around equilibrium points does not have a zero eigenvalue, see Izhikevich (2007), Khalil (2002), which holds in our case since the demand is an affine parameter of the system.

Consider a base case with $q_1 = 700$ [veh/h] and $q_2 = 650$ [veh/h], and the MFD parameters are the same as in example 1. Examples in Fig. 7 show the effect of different levels of endogenous and exogenous demands q_2 (Fig. 7a) and q_1 (Fig. 7b) in the size of the stable region, respectively. For all cases stable region is constructed for $u_{min} = 0.45$ and $u_{max} = 0.8$. Results in

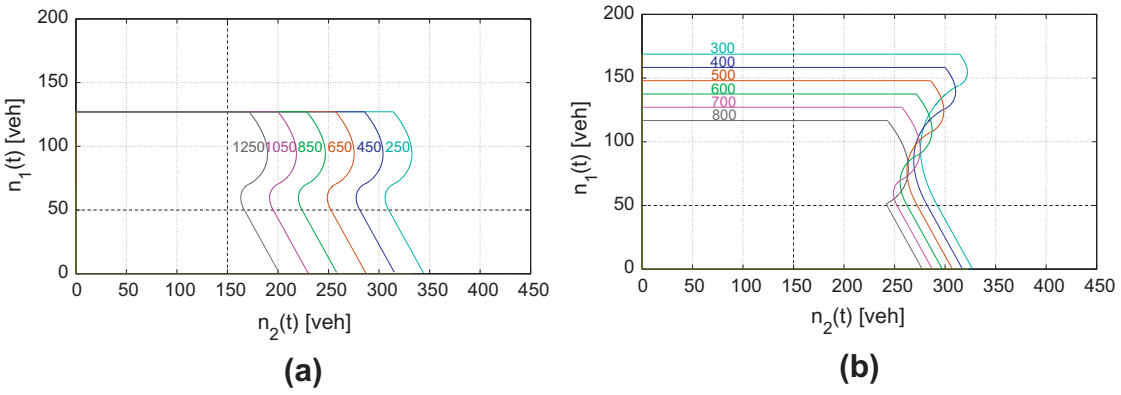

Fig. 7. Stable regions for different levels of (a) endogenous demand q_2 [veh/h], and (b) exogenous demand q_1 [veh/h].

Fig. 7a and b are as expected. The stable region becomes smaller as the number of trips with destinations to region 2 increases, then the system of the two regions will intend to be jammed, i.e. larger unstable region and smaller stable region.

4. State-feedback control for two-region MFDs

In this section, a stabilizing control solution is derived for the two-state two-region MFDs control problem (1)–(6). It will be shown in Section 4.1 that the two-region control problem is a feasibility (or stabilizing) problem, i.e. any feasible sequence of the perimeter control is an optimal solution, and all feasible solutions have the same value of the criterion for the same initial and end states, even when demands are time dependent. However, when the control problem has no feasible solution for the initial state, then the control cannot stabilize the two-region MFDs and the stable equilibrium end point is not reachable, hence, an optimal solution is derived for a relaxed problem as shown in Section 4.2.

4.1. Stabilizing control for feasibility control problem

First, let us assume that the two-region MFDs control problem has a feasible solution for the given initial state, i.e. at least one feasible solution $u(t)$ exists for $0 \leqslant t \leqslant t_f$, such that satisfies (6) and can bring initial states (4) to end states (5) in time duration t_f according to (2) and (3). In this case, one can integrate the differential Eqs. (2) and (3), and by summation one gets

$$n_{1,\mathrm{f}} + n_{2,\mathrm{f}} = \int_0^{t_\mathrm{f}} (q_1(t) + q_2(t))\mathrm{d}t - \int_0^{t_\mathrm{f}} G_2(n_2(t))\mathrm{d}t + n_{1,0} + n_{2,0}. \tag{21}$$

Note that $\int_0^{t_\mathrm{f}} G_2(n_2(t))\mathrm{d}t$ is the criterion to be optimized, see (1), hence substituting (1) into (21), one gets

$$J = \max_u \left(-n_{1,\mathrm{f}} - n_{2,\mathrm{f}} + \int_0^{t_\mathrm{f}} (q_1(t) + q_2(t))\mathrm{d}t + n_{1,0} + n_{2,0} \right), \tag{22}$$

which is equivalent to optimize:

$$J = \min_u (n_{1,\mathrm{f}} + n_{2,\mathrm{f}}). \tag{23}$$

Hence, (23) implies (1). When the end state is a priori known, then the criterion J is *independent* of $u(t)$ and the problem is a feasibility control problem: if any applied control $u(t)$ brings the initial state $(n_{2,0}, n_{1,0})$ to the end state $(n_{2,\mathrm{f}}, n_{1,\mathrm{f}})$ in time duration t_f where the initial state, end state, and t_f are a priori known, then the applied control $u(t)$ is optimal, in other words, all feasible controllers are also optimal. However, when the end point is assumed to be asymptotically a stable equilibrium point in stable region I, then according to (8) the sum of end state $n_{1,\mathrm{f}} + n_{2,\mathrm{f}}$ in (23) is minimized when the control sequence ends with $u(t_\mathrm{f}) = u_{\max}$.

Note that (22) is generally derived for any trajectory that moves and stays in the same region, i.e. $G_1(n_1(t))$ and $G_2(n_2(t))$ are the same functions for $0 \leqslant t \leqslant t_f$. However, it is easily shown that (22) holds also for trajectory that moves from one region to another while reaching the end state point. For example, let us consider a trajectory that moves through three state regions IV, III, and I, as shown in Fig. 8, where t_1 and t_2 the time instants when trajectory enters state region III and I, respectively. One can calculate the value of the criterion J_1 in region IV for $[0, t_1]$, and J_2 in region III for $[t_1, t_2]$, and J_3 in region I for $[t_2, t_f]$ according to (22), respectively,

$$J_1 = -n_1(t_1) - n_2(t_1) + \int_0^{t_1} (q_1(t) + q_2(t))\mathrm{d}t + n_{1,0} + n_{2,0}, \tag{24}$$

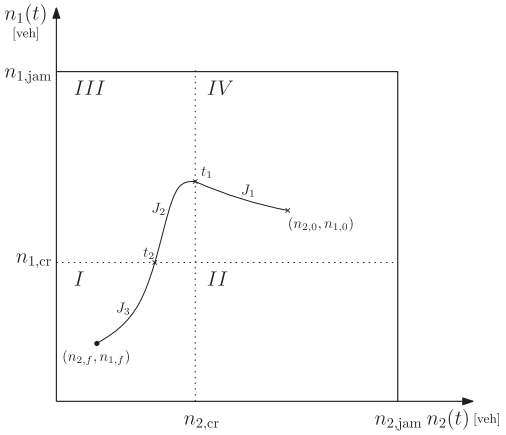

Fig. 8. Trajectory moves through three regions IV, III, and I.

$$J_2 = -n_1(t_2) - n_2(t_2) + \int_{t_1}^{t_2} (q_1(t) + q_2(t)), \mathrm{d}t + n_1(t_1) + n_2(t_1), \tag{25}$$

$$J_3 = -n_{1,\mathrm{f}} - n_{2,\mathrm{f}} + \int_{t_2}^{t_f} (q_1(t) + q_2(t))\mathrm{d}t + n_1(t_2) + n_2(t_2). \tag{26}$$

The value of the criterion J from 0 to t_f is calculated by summation of J_1 (24), J_2 (25), and J_3 (26), one gets (22). Hence, (22) holds for any trajectory that moves through different regions with different $G_1(n_1(t))$ and $G_2(n_2(t))$, and the problem is still a feasibility problem. Moreover, note that according to (22), the control problem is still a feasibility problem when demand varies with time. Instead of constant demand inside the integral, it will be substituted by time varying demand, which does not affect the derivation of (22).

However, the control problem may be not feasible for all initial states where the end state is not reachable, hence an optimal solution is derived for a relaxed problem where the end state is free.

4.2. Optimal control for relaxed control problem

When the two-state two-region control problem (1)–(6) has no feasible solution for the initial state, an optimal solution is derived for a relaxed control problem: two-state two-region control problem with free end state, i.e. (1)–(4), (6), and $(n_{2,\mathrm{f}}, n_{1,\mathrm{f}})$ is free. Note that for the relaxed problem, the assumption that control time horizon t_f is large enough to reach end state is dropped since the end state is free. The optimal relaxed control problems are solved separately for the four state regions in the (n_2, n_1)-plane correspond to $G_i(n_i(t))$, $i = 1, 2$, in each state region. The Pontryagin maximum principle (PMP) is used to solve the relaxed problems, see Pontryagin et al. (1962). In the following, the optimal solution is presented in details only for state region I, while the optimal solutions for the other three regions II, III, and IV are derived in a similar way.

For state region I, the *Hamiltonian*, denoted by H_I, is formed as

$$H_I = R_{1,\mathrm{I}} \cdot n_1(t) \cdot u(t) \cdot (p_2(t) - p_1(t)) + p_1(t) \cdot q_1 + p_2(t) \cdot (q_2 - R_{2,\mathrm{I}} \cdot n_2(t)) + R_{2,\mathrm{I}} \cdot n_2(t), \tag{27}$$

where $R_{1,\mathrm{I}} = \gamma_1/n_{1,\mathrm{cr}}$, $R_{2,\mathrm{I}} = \gamma_2/n_{2,\mathrm{cr}}$, and $p_1(t)$, $p_2(t)$ are the *costate* variables that satisfy

$$\frac{\mathrm{d}p_1}{\mathrm{d}t} = -\frac{\partial H}{\partial n_1} = R_{1,\mathrm{I}} \cdot u(t) \cdot (p_1(t) - p_2(t)), \tag{28}$$

$$\frac{\mathrm{d}p_2}{\mathrm{d}t} = -\frac{\partial H}{\partial n_2} = R_{2,\mathrm{I}} \cdot (p_2(t) - 1). \tag{29}$$

Recall that the end state $(n_2(t_f), n_1(t_f))$ is free, hence according to PMP it follows that $p_1(t_f) = 0$ and $p_2(t_f) = 0$. The Hamiltonian must be maximized over the control variable $u(t)$ subject to the control constraint (6). The optimal control solution obtained by $\max_u H$ in (27) is

$$u(t) = \begin{cases} u_{\max} & \text{if } p_2(t) - p_1(t) > 0, \\ u_{\min} & \text{if } p_2(t) - p_1(t) < 0. \end{cases} \tag{30}$$

A *switching point* t_s [sec] is the time instant that satisfies $p_2(t_s) = p_1(t_s)$. If there exists a switching point, then the optimal policy will be determined by that point.

The initial conditions of the costates should be chosen such that the resulting solution satisfies $p_1(t_f) = p_2(t_f) = 0$ and optimality condition (30). Note that if $p_2(0) > 1$ then $\mathrm{d}p_2/\mathrm{d}t > 0$, see (29), but this is a contradiction since $p_2(t_f) = 0$, hence lets assume that $p_2(t)$ is $0 \leqslant p_2(t) < 1$ and $p_1(0) > 0$. Since $p_1(t_f) = 0, p_1(t)$ must be decreasing for $0 \leqslant t < t_f$, i.e. $\mathrm{d}p_1/\mathrm{d}t < 0$, which implies $p_1(t) < p_2(t)$ for $0 \leqslant t < t_f$ according to (28), therefore the optimal control is $u(t) = u_{\max}$, see (30). In this case, there will be no switching point t_s otherwise $\mathrm{d}p_1/\mathrm{d}t > 0$ for $t_s \leqslant t \leqslant t_f$, however $p_1(t_f) = 0$ is not satisfied, therefore $t_s = t_f$.

The summary of optimal solutions for the relaxed problems is as follows, if the initial state $(n_{2,0}, n_{1,0})$ belongs to: state region I or III apply $u(t) = u_{\max}$, otherwise apply $u(t) = u_{\min}$ for state regions II and IV. In other words, when region 2 is in free-flow regime, one can increase the trip completion rate by increasing the region 2 flow. This can be realized by letting more vehicles entering the region and increasing the number of vehicles in the region to become closer to $n_{2,\mathrm{cr}}$, therefore, the perimeter control has to restrict minimum number of transferring vehicles from region 1 to region 2. On the contrary where region 2 is congested, any increase of $n_2(t)$ will decrease the flow and thus the trip completion, therefore, the perimeter control has to restrict maximum number of transferring vehicles in order to maximize the number of trips ended. This solution is exactly the same as proposed by Daganzo (2007) for a single region city. Nevertheless, this solution might not be optimal in case some trips have destination in region 1. We discuss this in Section 5.

4.3. State-feedback control strategy for time-dependent condition

A state-feedback control strategy is proposed according to the feasibility of two-region control problem (1)–(6), see Fig. 9a. If the necessary and sufficient conditions (12) and (13) hold, then the state space of the control problem is divided to stable and unstable regions, where for each region different state-feedback control is defined: a stabilizing state-feedback is applied for stable region to reach the optimal stable equilibrium point, and an optimizing state-feedback is applied for

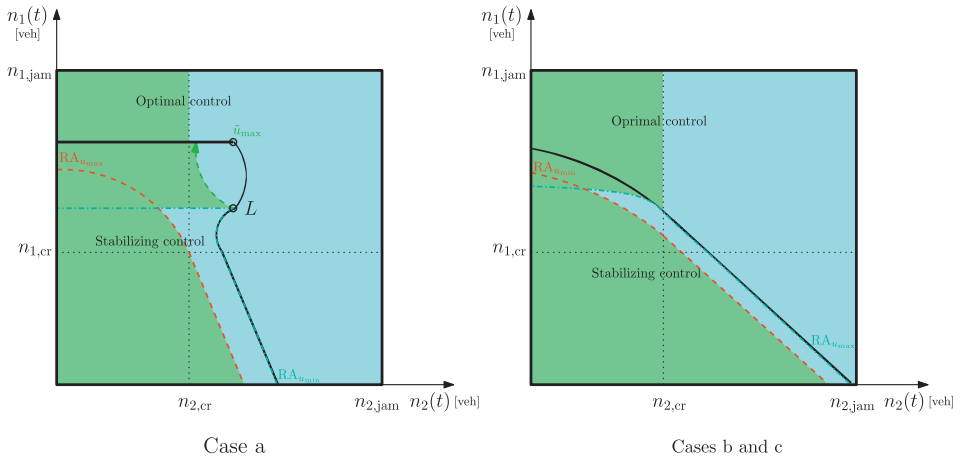

(a) State-feedback control for cases a, b, and c (green: apply $u_{\max}$, blue: apply $u_{\min}$)

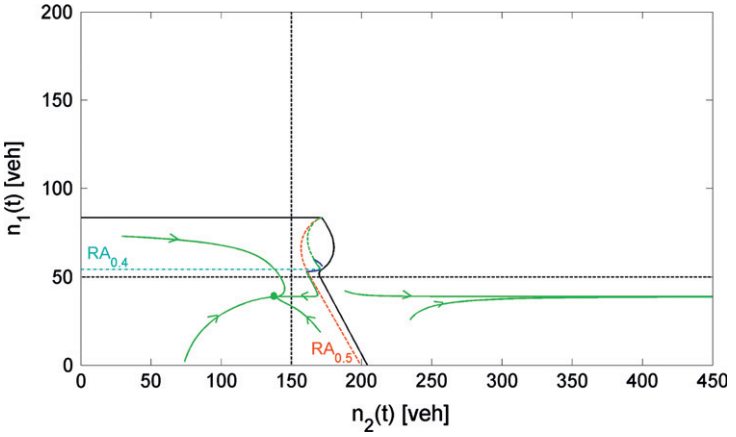

(b) Evolution of corresponding trajectories to state-feedback control strategy for example 5.

Fig. 9. State-feedback control strategy.

unstable region. The RA*s* are used in the two-state two-region control for stability characterization and state-feedback strategy.

The stabilizing state-feedback control depends on the $RA_{u_{\max}}$, $RA_{u_{\min}}$ and on $\tilde{u}_{\max}$ which is a reverse trajectory calculated with $u_{\max}$ starting from the equilibrium point in state region IV (11) for $u = u_{\min}$ (point L), see Fig. 9a case a. Note that it is not necessary that $\tilde{u}_{\max}$ trajectory ends in the corresponding equilibrium point of region IV (for $u = u_{\max}$), the trajectory continues until it hits the upper boundary of the stable region as shown in the figure.

The stabilizing state-feedback control is as follows: if the initial state belongs to the $RA_{u_{max}}$, then apply $u(t) = u_{\max}$ for $0 \leqslant t \leqslant t_f$ since it is proved that the value of the criterion is optimized with $u(t_f) = u_{\max}$, see Section 4.1. If the initial state does not belong to $RA_{u_{max}}$ but belongs to the $RA_{u_{\min}}$, then apply $u(t) = u_{\min}$ until the state trajectory enters the $RA_{u_{max}}$. If the initial state belongs to the stable region and does not belong to $RA_{u_{\max}}$ or $RA_{u_{\min}}$, then for case b or c apply $u(t) = u_{\max}$, however, for case a it depends on trajectory $\tilde{u}_{\max}$ which splits this region to two: (i) apply $u_{\max}$ for a point in region between $RA_{u_{\max}}$ and $\tilde{u}_{\max}$, and (ii) apply $u_{\min}$ for region between $\tilde{u}_{\max}$ and the border of stable region, see Fig. 9a. The state-feedback control strategy (n_2, n_1)-plane is demonstrated by example 5 with $u_{\max} = 0.5$, $u_{\min} = 0.4$ for several initial state points, as shown in Fig. 9b.

Note that when the demands are essentially nonconstant the state-feedback control solution can be used in the scheme of a predictive control by recalculating the stable region boundaries, $RA_{u_{\max}}$, $RA_{u_{min}}$, and the perimeter control at each new control step where the time varying demands can be approximated as constant demands for each control step.

Remark 1. If the necessary and sufficient conditions (12) and (13) for equilibrium points do not hold for the current demands, i.e. the system does not have a stable equilibrium point, the control problem (1)–(6) has no feasible solution for any $u(t)$ since the end point is defined as a stable equilibrium point. In this case, the optimal control solution is identical to

the relaxed problems and should be applied until the demands change with time such that the necessary and sufficient conditions (12) and (13) hold.

5. Region of attraction for three-state two-region system

In the previous section, a state-feedback solution is derived for the two-state two-region problem. This state-feedback strategy holds for more complicated two-region systems, e.g. in case some of the trips have destinations in both regions 1 and 2. However, the characterization of stable and unstable regions for three or four states system, is a tedious task but straightforward. Hence, in this paper only numerical results of RAs for three-state two-region system are presented, where trips generated from region 1 can finish in 1 or 2. Moreover, general guidance principles for the stability characterization and modifications of the state-feedback strategy are stated for the three-state system. The full stability analysis of the three-state two-region system will be a future research direction.

In the following, we deal with a traffic network that is partitioned into two regions $i = 1, 2$ and has three demands: two endogenous demand $q_{ii}(t)$ [veh/s], $i = 1, 2$, and one exogenous demand $q_{12}(t)$ [veh/s]. In this case, three accumulation states $n_{11}(t)$, $n_{12}(t)$, and $n_2(t)$ [veh] are used to model the dynamic equations, where $n_{11}(t)$ or $n_{12}(t)$ is the total number of vehicles in region (1) with destination (1) or (2) at time t, respectively, note that $n_1(t) = n_{11}(t) + n_{12}(t)$. The trip completion flow for region 1 is the sum of exit flow, i.e. trips from 1 with destination 2, plus the internal flow, i.e. trips from 1 with destination 1. The exit flow from 1 with destination to 2 is calculated correspondingly to the ratio between accumulations, i.e. $n_{12}/n_1 \cdot G_1(n_1(t))$, while the internal flow from 1 with destination to 1 is calculated by $n_{11}/n_1 \cdot G_1(n_1(t))$. These relationships assume that trip length for all trips within a region (internal or external) are similar. For a description in different case the reader can refer to Geroliminis (2009).

The control problem of the three-state two-region system is formulated as follows:

$$J = \max \int_0^{t_f} \left[\frac{n_{11}(t)}{n_1(t)} \cdot G_1(n_1(t)) + G_2(n_2(t)) \right] dt \tag{31}$$

subject to

$$\frac{dn_{11}(t)}{dt} = q_{11}(t) - \frac{n_{11}(t)}{n_{11}(t) + n_{12}(t)} \cdot G_1(n_1(t)), \tag{32}$$

$$\frac{dn_{12}(t)}{dt} = q_{12}(t) - \frac{n_{12}(t)}{n_{11}(t) + n_{12}(t)} \cdot G_1(n_1(t)) \cdot u(t), \tag{33}$$

$$\frac{dn_2(t)}{dt} = q_2(t) + \frac{n_{12}(t)}{n_{11}(t) + n_{12}(t)} \cdot G_1(n_1(t)) \cdot u(t) - G_2(n_2(t)), \tag{34}$$

$$n_{11}(0) = n_{11,0}; \quad n_{12}(0) = n_{12,0}; \quad n_2(0) = n_{2,0}, \tag{35}$$

$$n_{11}(t_f) = n_{11,f}; \quad n_{12}(t_f) = n_{12,f}; \quad n_2(t_f) = n_{2,f}, \tag{36}$$

$$0 < u_{min} \leqslant u(t) \leqslant u_{max} < 1. \tag{37}$$

Note that the optimization control problem for the three accumulation states (31)–(37) is also a feasibility problem. This can be proved in the same way as for the two-state problem, see Section 4.1.

Recall that the regions of attraction are utilized to characterize the stable and unstable regions. Computing the regions of attraction of an equilibrium point in the three-state system is more sophisticated than the two-state problem as there are three dimensional states (axes) instead of two. Hence, instead of computing a region boundary in a plane of two states, one has to compute a region surface boundary in a space of three states. The five steps presented in Section 3.1 for computing the region of attraction boundary for the two-state system can be extended to compute the surface boundary for the three-state system, however, analytical solutions cannot be easily obtained. Hence, the surface boundaries are numerically investigated for different splits and levels of demand through phase portraits computations in numerical example 6.

The input data for numerical example 6 are the same as example 1. However, the demand $q_1(t) = 0.194$ [veh/s] is split into two demands: $q_{11}(t) = 4/7 \cdot q_1(t)$ and $q_{12}(t) = 3/7 \cdot q_1(t)$. The boundary surfaces of $RA_{u_{max}}$ and $RA_{u_{min}}$ are shown in red and cyan colors, respectively, in Fig. 10a, and the corresponding trajectories to u_{max} are in green. This figure is analogous to Fig. 3d for the two-state example.

The surface boundary for the three-state problem is a collection of all boundary shapes in (n_{12}, n_2)-plane over all n_{11}, where $0 \leqslant n_{11} \leqslant n_{1,jam}$. The boundary shapes in (n_{12}, n_2)-plane are similar to the three boundary cases of the two-state system shown in Section 3.1. e.g. the $RA_{u_{max}}$ and $RA_{u_{min}}$ boundary shapes in (n_{12}, n_2)-plane with $n_{11} = 0$ in Fig. 10a are similar to those in Fig. 3d.

Fig. 10b and c show the effect of different splits of demand in region 1 on the $RA_{u_{max}}$. In Fig. 10b, the demand of region 1 is split to $q_{11}(t) = 2/3 \cdot q_1(t)$, while in Fig. 10c the split is reversed, i.e. $q_{11}(t) = 1/3 \cdot q_1(t)$. The total demand for regions 1 and 2 are $q_1(t) = 0.083$ [veh/s] and $q_2(t) = 0.472$ [veh/s], while the other input data are similar to those of example 6. Although the total demand q_1 is the same, the $RA_{u_{max}}$ shrinks when the exogenous demand $q_{12}(t)$ increases.

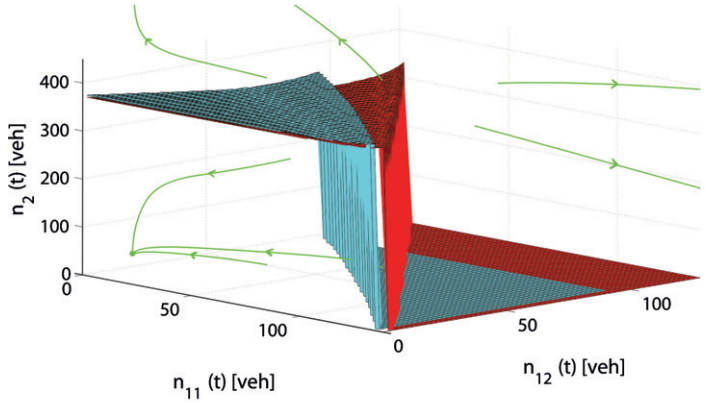

(a) Numerical example 6: RAs surface boundaries surfaces in three-state two-region system, $\mathrm{RA}_{u_{\max}}$ and $\mathrm{RA}_{u_{\min}}$ surface boundaries are drawn in red and cyan, respectively, and stable and unstable trajectories correspond to $u_{\max}$ are drawn in green.

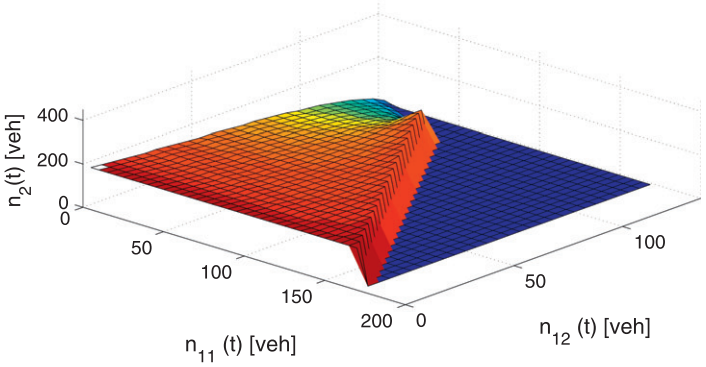

(b) $\mathrm{RA}_{u_{\max}}$ surface boundary for $q_{11}(t) = 2/3 \cdot q_1(t)$.

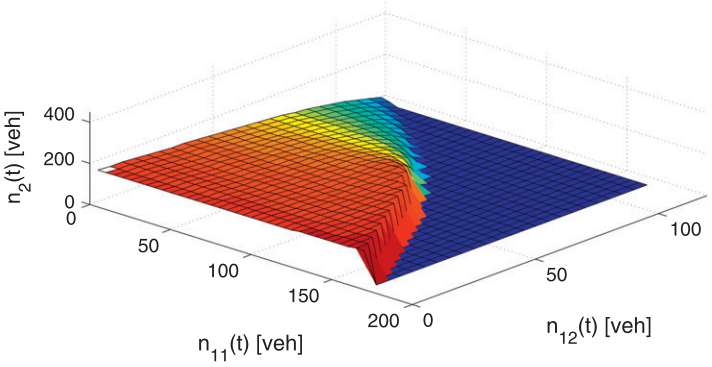

(c) $\mathrm{RA}_{u_{\max}}$ surface boundary $q_{11}(t) = 1/3 \cdot q_1(t)$.

Fig. 10. RAs surface boundaries. (For interpretation of the references to colour in this figure legend, the reader is referred to the web version of this article.)

In order to characterize the stable region, one should compute all region of attraction surface boundaries, and explore the state space outside all theses surface boundaries for trajectories that can enter inside one of the surface boundaries. This is a huge computational effort, while we believe that the same concept of the new algorithm introduced for the two-state holds also for the three-state system. This means that computing $\mathrm{RA}_{u_{\min}}$ surface boundary and a few trajectories is expected to be enough to characterize the stable region boundary. However, this area should be investigated more deeply in the future.

The stabilizing control of the state-feedback control strategy for the three-state system will also have the same concept presented for the two-state system in Section 4.1. Recall that the stabilizing control is applied when the current state, i.e. $n_{11}(t)$, $n_{12}(t)$, $n_2(t)$ in the three-state system, belongs to the stable region. If the state is inside the surface boundary of

$RA_{u_{max}}$ then one has to apply u_{max}, while if the state is outside the surface boundary of $RA_{u_{max}}$ but inside $RA_{u_{min}}$, then apply u_{min} until the trajectory enters $RA_{u_{max}}$. In the case when the state is outside both $RA_{u_{max}}$ and $RA_{u_{min}}$ surface boundaries, then choose $u(t)$ that brings the trajectory to enter one of the surface boundaries. However, this is the main issue as one has to apply a control that guaranties to bring the trajectory from these points to enter $RA_{u_{max}}$ or $RA_{u_{min}}$ surface boundary. This issue is unsolved yet and should be investigated more deeply in the future.

Regarding the optimal control for the relaxed control problem of three states is too tedious to be solved analytically by the Pontryagin Maximum Principle. However, instead of obtaining an analytical solution, the optimal control problem for the three-state and four-state system is solved in a state-feedback form using the model predictive control approach. For a detailed description the reader can refer to Haddad et al. (2012).

6. Conclusions

In this paper, the optimal control problem for two-region urban cities is formulated where the criterion is to maximize the number of vehicles that complete their trips and reach their destinations by controlling and managing accumulations in the two regions. The macroscopic fundamental diagram for each region is assumed to be known and in triangular shape. Later we relax this assumption and we investigate trapezoidal MFDs. In this paper, we analyze cases where one of the two regions is the center of attraction and does not generate exogenous demand. The first part focuses on systems where all trips have destination in the center of the city, while the second part allows some trips to remain outside the city center.

The dynamic equations of accumulations are analyzed, and equilibrium points of the system are identified. Necessary and sufficient conditions for existence of equilibrium points are derived. Based on the phase portraits of the dynamic equations, a new algorithm is presented to compute numerically and analytically the boundary between stable and unstable regions.

It is proven that the formulated control problem is a feasibility problem, i.e. if an applied control $u(t)$ brings the initial accumulations to a priori known optimal stable equilibrium accumulations, then $u(t)$ is an optimal perimeter control. However, if the problem is not feasible for the current accumulations, i.e. the current accumulations belong to unstable region, then the optimal control policy for a relaxed problem should be applied. Hence, based on the stable and unstable regions, a state-feedback strategy is proposed where the stabilizing (and optimizing) control law of the stable region and the optimal control law for the unstable region are presented in an analytical feedback form, as a function of the current accumulations. In the case when demands are essentially nonconstant this solution can be used in the scheme of a predictive control by recalculating region of attraction and control at each new step.

Future work involves the development of optimal control strategies for cities with more complex structures and different MFD shapes. Analytical solutions might be difficult to obtain under more complex cases, but decomposition of the system in not heavily interacting regions can be a solution. Control strategies that intervene on the demand side should also be considered (e.g. pricing, shift to more efficient and sustainable modes). These strategies would require a better understanding in the modeling of multi-modal systems where different modes of transport (buses, cars etc) interact for the same urban space.

Appendix A. Trajectory calculation of regions boundaries for cases a, b, and c

A.1. Case a

The trajectory from the unstable equilibrium point $(n_{2,eq}, n_{1,eq})_{IV}$ to point B (see Fig. 2) is calculated in reverse time (with negative t). Solution in reverse time is equivalent to solution in forward time (with positive t) of the dynamic equation

$$\frac{d\tilde{n}_1(t)}{dt} = -\frac{dn_1(t)}{dt}, \tag{A.1}$$

$$\frac{d\tilde{n}_2(t)}{dt} = -\frac{dn_2(t)}{dt}, \tag{A.2}$$

where $dn_1(t)/dt$ and $dn_2(t)/dt$ are the dynamic equations for state region IV, i.e. substituting (7) into the dynamic Eqs. (2) and (3) with $n_{1,cr} \leqslant n_1(t) \leqslant n_{1,jam}$ and $n_{2,cr} \leqslant n_2(t) \leqslant n_{2,jam}$. The direction of $(\tilde{n}_2(t), \tilde{n}_1(t))$ trajectory will be in reverse way, i.e from point B to the unstable equilibrium point $(n_{2,eq}, n_{1,eq})_{IV}$.

Given the initial state of the trajectory, i.e. $n_1(0) = n_{1,cr}$ and $n_2(0) = n_{2,B}$, where the starting time is zero, one can integrate (A.1) and (A.2), respectively,

$$\tilde{n}_1(t) = n_{1,jam} - \frac{q_1 \cdot (n_{1,jam} - n_{1,cr})}{\gamma_1 \cdot u} + (n_{1,jam} - n_{1,cr}) \cdot \left(\frac{q_1}{\gamma_1 \cdot u} - 1\right) \cdot e^{\frac{\gamma_1 \cdot u \cdot t}{\tilde{n}_{1,cr} - n_{1,jam}}}, \tag{A.3}$$

$$\tilde{n}_2(t) = \frac{e^{\frac{\gamma_1 \cdot u \cdot t}{\tilde{n}_{1,cr} - n_{1,jam}}} \cdot (q_1 - \gamma_1 \cdot u) \cdot (n_{1,cr} - n_{1,jam}) \cdot (n_{2,cr} - n_{2,jam})}{\gamma_2 \cdot (n_{1,jam} - n_{1,cr}) + \gamma_1 \cdot u \cdot (n_{2,cr} - n_{2,jam})} + \frac{n_{2,cr} \cdot (q_1 + q_2) + (\gamma_2 - q_1 - q_2) \cdot n_{2,jam}}{\gamma_2} + c_2 \cdot e^{\frac{\gamma_2 \cdot t}{\tilde{n}_{2,cr} - n_{2,jam}}}, \tag{A.4}$$

$$c_2 = \frac{\gamma_1 \cdot u \cdot (q_1 - \gamma_1 \cdot u) \cdot n_{1,\text{jam}} \cdot (n_{2,\text{cr}} - n_{2,\text{jam}})^2}{(\gamma_2 \cdot n_{1,\text{cr}} + \gamma_1 \cdot u \cdot (n_{2,\text{jam}} - n_{2,\text{cr}})) \cdot (\gamma_2 \cdot (n_{1,\text{cr}} - n_{1,\text{jam}}) + \gamma_1 \cdot u \cdot (n_{2,\text{jam}} - n_{2,\text{cr}}))}. \tag{A.5}$$

A.2. Case b

The trajectory from point C to B is in state region IV as shown in Fig. 2, hence the reverse equation system and the trajectory from B to C is the same as in case a, i.e. (A.3), (A.4), and (A.5).

For trajectory CD, the dynamic equations according to (A.1) and (A.2) are reversed where $dn_1(t)/dt$ and $dn_2(t)/dt$ are the dynamic equations for state region III, i.e. substituting (7) into the dynamic Eqs. (2) and (3) with $n_{1,\text{cr}} \leqslant n_1(t) \leqslant n_{1,\text{jam}}$ and $0 \leqslant n_2(t) \leqslant n_{2,\text{cr}}$. The direction of $(\tilde{n}_2(t), \tilde{n}_1(t))$ trajectory will be in reverse way, i.e from C to D. Given the initial state of the trajectory CD, i.e. $n_1(0) = n_{1,C}$ and $n_2(0) = n_{2,\text{cr}}$, where the starting time is zero, one can integrate (A.1) and (A.2), respectively,

$$\tilde{n}_1(t) = \frac{n_{1,\text{cr}} \cdot q_1 - q_1 \cdot n_{1,\text{jam}} + \gamma_1 \cdot u \cdot n_{1,\text{jam}}}{\gamma_1 \cdot u} + \left(n_{1,C} - n_{1,\text{jam}} - \frac{q_1 \cdot (n_{1,\text{cr}} - n_{1,\text{jam}})}{\gamma_1 \cdot u} \right) \cdot e^{\frac{\gamma_1 \cdot u \cdot t}{n_{1,\text{cr}} - n_{1,\text{jam}}}}, \tag{A.6}$$

$$\tilde{n}_2(t) = n_{2,\text{cr}} \cdot \left(\frac{q_1 + q_2}{\gamma_2} + \frac{e^{\frac{\gamma_1 \cdot u \cdot t}{n_{1,\text{cr}} - n_{1,\text{jam}}}} \cdot (n_{1,\text{cr}} \cdot q_1 - q_1 \cdot n_{1,\text{jam}} + \gamma_1 \cdot u \cdot (n_{1,\text{jam}} - n_{1,C}))}{\gamma_1 \cdot n_{2,\text{cr}} \cdot u + \gamma_2 \cdot (n_{1,\text{jam}} - n_{1,\text{cr}})} \right) + c_2 \cdot e^{\frac{\gamma_2 \cdot t}{n_{2,\text{cr}}}}, \tag{A.7}$$

$$c_2 = n_{2,\text{cr}} \cdot \left(1 - \frac{q_1 + q_2}{\gamma_2} - \frac{q_1 \cdot (n_{1,\text{cr}} - n_{1,\text{jam}}) + \gamma_1 \cdot u \cdot (n_{1,\text{jam}} - n_{1,C})}{\gamma_1 \cdot n_{2,\text{cr}} \cdot u + \gamma_2 \cdot (n_{1,\text{jam}} - n_{1,\text{cr}})} \right). \tag{A.8}$$

The curves BC and CD for case b are calculated according to the following steps:

1. find T_{BC} [sec] the time instant when trajectory BC enters state region III, i.e. solve numerically $\tilde{n}_2(T_{BC}) = n_{2,\text{cr}}$, where $\tilde{n}_2(t)$ is given by (A.4) and (A.5),
2. calculate trajectory BC, i.e. calculate $(\tilde{n}_1(t), \tilde{n}_2(t))$ for $t = 0 \rightarrow T_{BC}$ according to (A.3), (A.4), and (A.5),
3. save point $C = (n_{2,C}, n_{1,C}) = (n_{2,\text{cr}}, \tilde{n}_1(T_{BC}))$,
4. find T_{CD} [sec] the time instant when trajectory CD intersects $n_2(t) = 0$, i.e. solve numerically $\tilde{n}_2(T_{CD}) = 0$, where $\tilde{n}_2(t)$ is given by (A.7) and (A.8),
5. calculate trajectory CD, i.e. calculate $(\tilde{n}_1(t), \tilde{n}_2(t))$ for $t = 0 \rightarrow T_{CD}$ according to (A.6), (A.7), and (A.8).

A.3. Case c

In this case, the trajectory BC is in state region I as shown in Fig. 2. Hence, given the initial state of the trajectory BC, i.e. $n_1(0) = n_{1,B}$ and $n_2(0) = n_{2,\text{cr}}$, where the starting time is zero, one can integrate (A.1) and (A.2), respectively, where $dn_1(t)/dt$ and $dn_2(t)/dt$ are the dynamic equations for state region I, i.e. substituting (7) into the dynamic Eqs. (2) and (3) with $0 \leqslant n_1(t) \leqslant n_{1,\text{cr}}$ and $0 \leqslant n_2(t) \leqslant n_{2,\text{cr}}$,

$$\tilde{n}_1(t) = \frac{n_{1,\text{cr}} \cdot q_1}{\gamma_1 \cdot u} + \left(n_{1,B} - \frac{n_{1,\text{cr}} \cdot q_1}{\gamma_1 \cdot u} \right) \cdot e^{\frac{\gamma_1 \cdot u \cdot t}{n_{1,\text{cr}}}}, \tag{A.9}$$

$$\tilde{n}_2(t) = n_{2,\text{cr}} \cdot \left(\frac{q_1 + q_2}{\gamma_2} + \frac{e^{\frac{\gamma_1 \cdot t \cdot u}{n_{1,\text{cr}}}} \cdot (-n_{1,\text{cr}} \cdot q_1 + \gamma_1 \cdot n_{1,B} \cdot u)}{\gamma_2 \cdot n_{1,\text{cr}} - \gamma_1 \cdot n_{2,\text{cr}} \cdot u} \right) + c_2 \cdot e^{\frac{\gamma_2 \cdot t}{n_{2,\text{cr}}}}, \tag{A.10}$$

$$c_2 = n_{2,\text{cr}} \cdot \left(1 - \frac{q_1 + q_2}{\gamma_2} - \frac{\gamma_1 \cdot n_{1,B} \cdot u - n_{1,\text{cr}} \cdot q_1}{\gamma_2 \cdot n_{1,\text{cr}} - \gamma_1 \cdot n_{2,\text{cr}} \cdot u} \right). \tag{A.11}$$

It holds for point C that $\tilde{n}_1(T_{BC}) = n_{1,\text{cr}}$, hence, from (A.9) one can calculate analytically T_{BC}

$$T_{BC} = \ln \left(\frac{n_{1,\text{cr}} \cdot (1 - \frac{q_1}{\gamma_1 \cdot u})}{n_{1,B} - \frac{q_1}{\gamma_1 \cdot u}} \right) \cdot \frac{q_1}{\gamma_1 \cdot u}. \tag{A.12}$$

The trajectory CD is calculated in the same way that was done in case b, however with different initial state. The dynamic equations are reversed according to (A.1) and (A.2) where, $dn_1(t)/dt$ and $dn_2(t)/dt$ are the dynamic equations for state region III, i.e. substituting (7) into the dynamic Eqs. (2) and (3) with $n_{1,\text{cr}} \leqslant n_1(t) \leqslant n_{1,\text{ jam}}$ and $0 \leqslant n_2(t) \leqslant n_{2,\text{cr}}$. Given the initial state of the trajectory CD, $n_1(0) = n_{1,\text{cr}}$ and $n_2(0) = \tilde{n}_2(T_{BC})$, where the starting time is zero, one can integrate (A.1) and (A.2), respectively, and one get same equations as in case b, i.e. (A.6) and (A.7), where c_2 is slightly different:

$$c_2 = n_{2,C} - n_{2,\mathrm{cr}} \cdot \left(\frac{q_1 + q_2}{\gamma_2} + \frac{q_1 \cdot (n_{1,\mathrm{cr}} - n_{1,\mathrm{jam}}) + \gamma_1 \cdot u \cdot (n_{1,\mathrm{jam}} - n_{1,\mathrm{cr}})}{\gamma_1 \cdot n_{2,\mathrm{cr}} \cdot u + \gamma_2 \cdot (n_{1,\mathrm{jam}} - n_{1,\mathrm{cr}})} \right). \tag{A.13}$$

The curves *BC* and *CD* for case c are calculated according to the following steps:

1. $B = (n_{2,\mathrm{cr}}, n_{1,B})$,
2. calculate analytically T_{BC} according to (A.12),
3. calculate trajectory *BC*, i.e. calculate $(\tilde{n}_1(t), \tilde{n}_2(t))$ for $t = 0 \rightarrow T_{BC}$ according to (A.9)–(A.11),
4. save point $C = (n_{2,C}, n_{1,C}) = (\tilde{n}_1(T_{BC}), n_{1,\mathrm{cr}})$,
5. find T_{CD} [sec] the time instant when trajectory *CD* intersects $n_2(t) = 0$, i.e. solve numerically $\tilde{n}_2(T_{CD}) = 0$, where $\tilde{n}_2(t)$ is given by (A.7) and (A.13),
6. calculate trajectory *CD*, i.e. calculate $(\tilde{n}_1(t), \tilde{n}_2(t))$ for $t = 0 \rightarrow T_{CD}$ according to (A.6), (A.7), and (A.13).

Note that if the trajectory starting from point *B* hits $n_2(t) = 0$ before entering region III, then in this case there is no curve *CD*.

References

Bemporad, A., Ferrari-Trecate, G., Morari, M., 2000. Observability and controllability of piecewise affine and hybrid systems. IEEE Transactions on Automatic Control 45 (10), 1864–1876.

Boyacı, B., Geroliminis, N., 2011. Exploring the effect of variability of urban systems characteristics in the network capacity. In: Transportation Research Board Annual Meeting, Washington, DC.

Buisson, C., Ladier, C., 2009. Exploring the impact of homogeneity of traffic measurements on the existence of macroscopic fundamental diagrams. Transportation Research Record 2124, 127–136.

Chiang, H.-D., Thorp, J.S., 1989. Stability regions of nonlinear dynamical systems: a constructive methodology. IEEE Transactions on Automatic Control 34 (12), 1229–1241.

Courbon, T., Leclercq, L., 2011. Cross-comparison of macroscopic fundamental diagram estimation methods. In: 14th EWGT Meeting – In Quest for Advanced Models, Tools and Methods for Transportation/Logistics.

Daganzo, C.F., 2007. Urban gridlock: macroscopic modeling and mitigation approaches. Transportation Research Part B 41 (1), 49–62.

Daganzo, C.F., Gayah, V.V., Gonzales, E.J., 2011. Macroscopic relations of urban traffic variables: bifurcations, multivaluedness and instability. Transportation Research Part B 45 (1), 278–288.

Daganzo, C.F., Geroliminis, N., 2008. An analytical approximation for the macroscopic fundamental diagram of urban traffic. Transportation Research Part B 42 (9), 771–781.

Elliott, D.L., 2009. Bilinear Control Systems. Springer.

Geroliminis, N., 2009. Dynamics of peak hour and effect of parking for congested cities. In: Transportation Research Board Annual Meeting, No. 09-1685, Washington, DC.

Geroliminis, N., Daganzo, C.F., 2008. Existence of urban-scale macroscopic fundamental diagrams: some experimental findings. Transportation Research Part B 42 (9), 759–770.

Geroliminis, N., Sun, J., 2011. Properties of a well-defined macroscopic fundamental diagram for urban traffic. Transportation Research Part B 45 (3), 605–617.

Godfrey, J.W., 1969. The mechanism of a road network. Traffic Engineering and Control 11 (7), 323–327.

Gutman, P.-O., 1981. Stabilizing controllers for bilinear systems. IEEE Transactions on Automatic Control 26 (4), 917–922.

Haddad, J., Ramezani, M., Geroliminis, N., 2012. Model predictive perimeter-control for two-region urban cities. In: Transportation Research Board Annual Meeting, No. 12-1445, Washington, DC.

Hassibi, A., Boyd, S., 1998. Quadratic stabilization and control of piecewise-linear systems. In: the American Control Conference, pp. 3659–3664.

Herman, R., Prigogine, I., 1979. A two-fluid approach to town traffic. Science 204 (4389), 148–151.

Izhikevich, E.M., 2007. Dynamical Systems in Neuroscience: The Geometry of Excitability and Bursting. The MIT press.

Ji, Y., Daamen, W., Hoogendoorn, S., Hoogendoorn-Lanser, S., Qian, X., 2010. Macroscopic fundamental diagram: investigating its shape using simulation data. Transportation Research Record 2161, 42–48.

Ji, Y., Geroliminis, N., 2011. Spatial and temporal analysis of congestion in urban transportation networks. In: Transportation Research Board Annual Meeting, Washington, DC.

Johansson, M., Rantzer, A., 1998. Computation of piecewise quadratic Lyapunov functions for hybrid systems. IEEE Transactions on Automatic Control 43 (4), 555–559.

Kalman, R.E., 1960. Contributions to the theory of optimal control. Boletin Sociedad Matematica Mexicana 5, 102–119.

Khalil, H.K., 2002. Nonlinear Systems, third ed. Prentice Hall.

Laval, L., 2010. The effect of signal timing and network irregularities in the macroscopic fundamental diagram. In: Traffic Flow Theory Summer Meeting, Annecy, France.

Mazloumian, A., Geroliminis, N., Helbing, D., 2010. The spatial variability of vehicle densities as determinant of urban network capacity. Philosophical Transactions of the Royal Society A: Mathematical, Physical and Engineering Sciences 368 (1928), 4627–4647.

Mhaskar, P., El-Farra, N.H., Christofides, P.D., 2006. Stabilization of nonlinear systems with state and control constraints using Lyapunov-based predictive control. Systems and Control Letters 55 (8), 650–659.

Pontryagin, L., Boltyanskii, V., Gamkrelidze, R., Mishchenko, E., 1962. The Mathematical Theory of Optimal Processes. Wiley-Interscience, NY.

Sastry, S., 1999. Nonlinear Systems: Analysis, Stability, and Control. Springer.

Tan, W., Packard, A., 2008. Stability region analysis using polynomial and composite polynomial Lyapunov functions and sum-of-squares programming. IEEE Transactions on Automatic Control 53 (2), 565–571.

Topcu, U., Packard, A., 2009. Local stability analysis for uncertain nonlinear systems. IEEE Transactions on Automatic Control 54 (5), 1042–1047.